HHS Public Access

Author manuscript

Nature. Author manuscript; available in PMC 2021 January 07.

Published in final edited form as:

Nature. 2020 April ; 580(7805): 647–652. doi:10.1038/s41586-020-2174-3.

AIM2 inflammasome surveillance of DNA damage shapes neurodevelopment

Catherine R. Lammert[1,2], **Elizabeth L. Frost**[1], **Calli E. Bellinger**[1], **Ashley C. Bolte**[1,3,4], **Celia A. McKee**[1], **Mariah E. Hurt**[1], **Matt J. Paysour**[1], **Hannah E. Ennerfelt**[1,2], **John R. Lukens**[1,2,*]

[1]Center for Brain Immunology and Glia (BIG), Department of Neuroscience, School of Medicine, University of Virginia, Charlottesville, VA 22908, USA.

[2]Neuroscience Graduate Program, School of Medicine, University of Virginia, Charlottesville, VA 22908, USA.

[3]Medical Scientist Training Program, School of Medicine, University of Virginia, Charlottesville, VA 22908, USA.

[4]Immunology Training Program, School of Medicine, University of Virginia, Charlottesville, VA 22908, USA.

Abstract

Neurodevelopment is characterized by rapid rates of neural cell proliferation and differentiation followed by a period of massive cell death where over half of all recently generated brain cells are pruned back. Large amounts of DNA damage, cellular debris, and byproducts of cellular stress are generated during these neurodevelopmental events, all of which can potentially activate immune signaling. How the immune response to this collateral damage influences brain maturation and function currently remains poorly understood. Here we show that the AIM2 inflammasome contributes to proper brain development and that disruptions in this immune sensor of genotoxic stress lead to behavioral abnormalities. The AIM2 inflammasome has been most extensively studied in the context of infection, where its activation in response to double-stranded DNA (dsDNA) is known to trigger cytokine production as well as a Gasdermin-D-mediated form of cell death commonly referred to as pyroptosis[1–4]. We observe pronounced AIM2 inflammasome activation in neurodevelopment and find that defects in this DNA damage surveillance sensor result in anxiety-related behaviors. We further show that the AIM2 inflammasome contributes to central nervous system (CNS) homeostasis specifically through its regulation of the cell death executioner Gasdermin-D, and not via its involvement in IL-1 and/or IL-18 production. Consistent with a role for this sensor of genomic stress in the purging of genetically compromised CNS cells, we find that defective AIM2 inflammasome signaling results in decreased neural cell death both in response to DNA damage-inducing agents and during neurodevelopment. Moreover, we report that

[*]**Correspondence should be addressed to:** John R. Lukens, Department of Neuroscience, Center for Brain Immunology and Glia, University of Virginia, 409 Lane Road, MR4- 6154, Charlottesville VA 22908, Tel: 434-984-7782, Fax: 434-982-4380, Jrl7n@virginia.edu.

Contributions

C.R.L. and J.R.L. designed the study; C.R.L., E.L.F., C.E.B., A.C.B., C.A.M., M.E.H., M.J.P., H.E.E., and J.R.L. performed experiments; C.R.L. and J.R.L. analyzed data and wrote the manuscript; J.R.L. oversaw the project.

Competing Interests

The authors declare no competing financial interests

disruptions in DNA damage surveillance by the AIM2 inflammasome lead to excessive DNA damage accumulation in neurons as well as increased numbers of neurons that incorporate into the adult brain. Our findings identify the inflammasome as a critical player in establishing a properly formed CNS through its role in the removal of genetically compromised cells.

Keywords

AIM2 inflammasome; neuroimmunology; DNA damage; neurodevelopment; behavior; Gasdermin-D; pyroptosis; CNS cell death; neural cell pruning; anxiety

Here we asked whether the damage signals generated during neurodevelopment trigger activation of the innate immune response and, if so, how this immune activation shapes neurodevelopment and behavior. The high levels of replicative stress and cell death that occur during brain maturation are known to generate a number of damage/danger signals such as DNA damage, ATP, and mitochondrial stress, all of which are capable of triggering inflammasome activation. Inflammasomes are multiprotein complexes that generally consist of an intracellular receptor such as NLRP3 or AIM2, the adaptor protein ASC, and the enzyme Caspase-1. Formation of this innate immune signaling platform coordinates Caspase-1 activation which can subsequently promote IL-1 and IL-18 production, as well as a Gasdermin-D-mediated form of cell death commonly referred to as pyroptosis.

ASC specks form in neurodevelopment

Since both cytokine production and cell death have been shown to be pivotal modulators of neurodevelopment[5–14], along with the fact that key inflammasome components are highly expressed during developmental time points (Extended Data Fig. 1a–c), we were interested in determining if inflammasome activation influences brain maturation and CNS function. We first asked if inflammasome activation is observed during neurodevelopment. To test this, we utilized ASC reporter mice to track the development of ASC specks, which is a prototypical marker of inflammasome activation[15]. When we looked in the developing brain at postnatal day 5 (p5), a time point characterized by high levels of DNA damage and cell death[16,17], we observed surprisingly high levels of ASC speck formation throughout the brain (Fig. 1a–b and Extended Data Fig. 2a). In comparison, we were barely able to detect any ASC specks in fully matured lymphoid organs such as the lymph nodes (LNs) (Fig. 1b and Extended Data Fig. 2b–c).

Inflammasomes influence behavior

We next wanted to assess the importance of inflammasome activation in setting up a properly functioning CNS. To accomplish this, we performed a battery of behavioral tests on Caspase-1/11-deficient mice (also referred to as *Ice*$^{-/-}$ mice*).* We found that genetic ablation of the inflammasome results in profound anxiety-like behaviors in the elevated plus maze and in open field testing (Fig. 1c–g). More specifically, we observed that *Ice*$^{-/-}$ mice spent significantly less time exploring the open arm of the elevated plus maze (Fig. 1c–d). Moreover, in open field testing, *Ice*$^{-/-}$ mice explored the center significantly less than WT mice, urinated more frequently, and produced more fecal pellets (Fig. 1e–g and Extended

Data Fig. 3a–b). To ensure that impaired vision and/or locomotor activity did not underlie the poor performance of inflammasome-deficient mice in our behavioral tests, we evaluated their ability to find a visible escape platform in the Morris water maze (MWM). In these studies, deletion of the inflammasome was not found to negatively impact the ability of mice to reach the visual platform indicating that neither impaired vision nor motor deficits likely contribute to the differences in performance seen in our elevated plus and open field tests (Fig. 1h). Genetic ablation of inflammasome signaling in Caspase-1/11-deficient mice also did not result in global behavioral abnormalities as *Ice*$^{-/-}$ mice were found to perform normally in the tail suspension and sucrose preference tests (Extended data Fig. 3c–d), both of which are commonly used to assess depressive behaviors. Collectively these results indicate that impaired inflammasome activation leads to behavioral abnormalities that include the development of pronounced anxiety-like behaviors.

The immune system is equipped with a repertoire of intracellular receptors that enable the host to coordinate inflammasome activation in response to a diverse array of pathogens and endogenous damage/danger signals. We first turned our attention to a potential role for NLRP3 in our model, as NLRP3 is known to incite inflammasome activation in response to a diverse array of damage/danger-associated molecular patterns (DAMPs) that are likely generated during normal brain maturation (e.g., ATP, damaged mitochondria, reactive oxygen species, etc.)[4]. To our initial surprise, we found that *Nlrp3*$^{-/-}$ mice performed similar to WT mice in the elevated plus maze, open field, visual platform test, and depressive assays (Fig.1 c–h, Extended Data Fig. 3). These results suggest that NLRP3 is not coordinating the inflammasome activation needed to prevent the development of anxiety-like behaviors in mice.

The AIM2 inflammasome impacts behavior

Maintenance of genomic integrity is essential for CNS health and mounting evidence suggests that inability to control genotoxic stress centrally contributes to a number of neurodevelopmental, psychiatric, and neurodegenerative disorders[18,19]. In the majority of cases, DNA damage is quickly remediated by repair pathways. However, DNA insults can persist as a result of unsuccessful repair attempts and/or impaired DNA damage removal[20,21]. Recent studies conducted in peripheral immune cells have shown that sensing of DNA damage by AIM2 can trigger inflammasome activation[22]. In addition, emerging work has described roles for AIM2 in models of CNS injury[23,24] and also has begun to characterize how deletion of AIM2 can alter neuronal morphology and influence behavior[25]. However, it still remains to be determined whether the AIM2 inflammasome is activated during neurodevelopment and, if so, how this impacts brain maturation and behavior. When we tested AIM2-deficient mice for anxiety-like behaviors we found that *Aim2*$^{-/-}$ mice phenocopied *Ice*$^{-/-}$ mice and displayed anxiety-like behaviors in both the elevated plus maze and the open field test (Fig. 1c–g, Extended Data Fig. 3a–b). Like *Ice*$^{-/-}$ mice, AIM2-deficient mice reached the visual platform in the MWM in similar times as their WT controls (Fig. 1h) and performed normally in both the tail suspension and sucrose preference tests (Extended Data Fig. 3c–d).

DNA damage and AIM2 promote ASC specks

Since key AIM2 inflammasome-associated genes are abundantly expressed during neurodevelopment (Extended Data Fig. 1) and dsDNA is known to activate AIM2, we were next interested in elucidating whether the DNA damage that normally arises during neurodevelopment can trigger AIM2 inflammasome activation in the developing brain. As a first approach, we explored if the inflammasome activation observed during neurodevelopment occurs in close proximity to cells harboring DNA damage. To this end, we evaluated the spatial localization of ASC specks in relation to cells that co-stain for the DNA damage markers γH2AX and 53BP1. Many of the ASC specks formed in the developing brain were identified to be in the vicinity of cells that co-stained for the DNA damage markers γH2AX and 53BP1 (Extended Data Fig. 4a). Moreover, we found that the bulk of this inflammasome activation at p5 in neurodevelopment is dependent on AIM2 surveillance, as genetic abrogation of AIM2 greatly decreased the number of ASC specks detected in the developing cerebellum (Fig. 1i–j). To further interrogate whether the AIM2 inflammasome can be activated in the developing brain in response to DNA damage, we induced overt DNA damage at p5 in the brains of WT and AIM2-deficient mice by exposing them to ionizing radiation (IR). We found that exposure to ionizing radiation results in increased expression of DNA damage markers in WT mice (i.e. γH2AX staining) and that this corresponds with concomitant increases in inflammasome activation (ASC speck formation) (Extended Data Fig. 4b–e). We observed a corresponding increase in γH2AX staining in ionizing radiation-treated AIM2-deficient mice (Extended Data Fig. 4b–c). However, ASC speck formation was substantially blunted in the absence of AIM2 (Extended Data Fig. 4d–e). Taken together, these findings suggest that AIM2 inflammasome activation occurs during neurodevelopment likely in response to DNA damage and that disruptions in this pathway can lead to behavioral abnormalities.

Gasdermin-D shapes behavior

Inflammasome activation can lead to IL-1 and IL-18 secretion, as well as a Gasdermin-D-mediated form of cell death, both of which can potentially impact neurodevelopment and behavior. Cytokines have been shown to be pivotal modulators of neurodevelopment, CNS function, and behavior[5,6,8–10]. In particular, the inflammasome-derived cytokines IL-1 and IL-18 have been reported to have especially prominent effects on the CNS[6,8–10]. Therefore, we were interested in discerning whether the observed behavioral abnormalities in AIM2 inflammasome-deficient mice were caused by disruptions in AIM2 inflammasome-mediated production of IL-1 and/or IL-18. Surprisingly, abrogation of IL-1 or IL-18 signaling were not found to promote anxiety-related phenotypes (Fig. 2a–b, Extended Data Fig. 5a–c). To interrogate whether IL-1 and IL-18 can play compensatory roles in shaping behavior, we also evaluated anxiety-related phenotypes in mice that lack MYD88, which is an essential adaptor molecule required for both IL-1R and IL-18R signaling. However, abrogation of MYD88 signaling was not observed to influence performance in tests measuring anxiety-related behaviors (Fig. 2a–b, Extended Data Fig. 5a–e).

In addition to orchestrating IL-1 and IL-18 production, AIM2 inflammasome activation can also incite a Gasdermin-D-mediated form of cell death. To explore the role that Gasdermin-

D plays in driving anxiety-like phenotypes, we assessed the performance of Gasdermin-D knockout mice in the elevated plus maze. Similar to *Ice*$^{-/-}$ and *Aim2*$^{-/-}$ mice (Fig. 1c–d), Gasdermin-D-deficient mice spent less time exploring the open arm of the elevated plus maze (Fig. 2c–d). Caspase-11, like Caspase-1, is also to known to orchestrate Gasdermin-D activation through noncanonical inflammasome signaling[26]. Nevertheless, Caspase-11-deficient mice were found to perform similarly to WT mice in both elevated-plus maze and open field testing (Fig. 2c–d, Extended Data Fig. 5f–h). Taken together, these results suggest that the behavioral abnormalities observed in AIM2 inflammasome-deficient mice are likely not due to defects in Caspase-1-mediated production of IL-1 and/or IL-18, but rather result from impaired Gasdermin-D signaling.

AIM2 coordinates neural cell death

It is believed that upwards of half of all neural cells are eliminated during neurodevelopment[11]. This process of neural cell pruning plays beneficial roles in the sculpting of strong connections in the brain and, consistent with this idea, disruptions in CNS cell death during development have been shown to cause neurological dysfunction[11–14]. Neuronal dieback is thought to occur solely through apoptotic cell death; however, this requires revisiting with the recent discovery of other forms of programmed cell death that include pyroptosis, necroptosis, and autophagic cell death[27]. Given our data indicating that the cell death executioner Gasdermin-D and the DNA damage sensor AIM2 both play key roles in limiting neurological dysfunction, we speculated that AIM2 inflammasome-induced cell death may help to prevent genetically compromised cells from being incorporated into the mature brain. To explore this possibility, we first evaluated if AIM2 inflammasome signaling is involved in CNS cell turnover in response to endogenous DNA damage. To this end, mixed cortical neural cells from WT, *Aim2*$^{-/-}$, *Ice*$^{-/-}$, and *Gsdmd*$^{-/-}$ mice were either transfected with dsDNA (PolydA:dT) as a positive control or treated with ionizing radiation or the topoisomerase II inhibitor, etoposide, to induce endogenous DNA damage. We detected a substantial reduction in DNA damage-induced cell death in CNS cells lacking AIM2, Caspase-1/11, or Gasdermin-D (Fig. 3a–b, Extended Data Fig. 6a–b).

To investigate whether the AIM2 inflammasome plays a role in coordinating neural cell dieback *in vivo*, we evaluated cell death in the cerebellum of WT and AIM2 inflammasome-deficient mice at p5, as this region of the brain has been previously reported to undergo DNA damage-induced cell death at this timepoint in neurodevelopment[16,17]. We find that genetic ablation of AIM2 leads to reduced levels of cell death as indicated by a decrease in TUNEL and propidium iodide (PI)-positive cell staining in the cerebellums of p5 *Aim2*$^{-/-}$ mice (Fig. 3c, Extended Data Fig. 7a–c). A reduction in cell death was also seen in *Casp1/11*$^{-/-}$ and *Gsdmd*$^{-/-}$ p5 cerebellums, indicating that the AIM2 inflammasome and Gasdermin-D are involved in orchestrating cell death at p5 in the developing brain (Fig. 3c, Extended Data Fig. 7a). Notably, disruptions in AIM2 inflammasome signaling were not found to completely abrogate levels of CNS cell death at this timepoint, suggesting that other forms of cell death including apoptosis are also contributing to CNS cell pruning in AIM2 inflammasome-deficient mice. To further test our working model, which proposes that AIM2 inflammasome signaling coordinates the removal of DNA damage harboring CNS

cells, we induced overt DNA damage in the developing brains of WT and AIM2-deficient mice by exposing them to ionizing radiation. We found that exposure to ionizing radiation results in increased TUNEL staining in WT and *Aim2*$^{-/-}$ mice; however, IR-induced cell death was substantially blunted in the absence of AIM2 (Extended Data Fig. 7d–e). These findings suggest that AIM2 is capable of executing cell death in response to IR-driven DNA damage.

AIM2 limits DNA damage levels in the CNS

If the AIM2 inflammasome does indeed function in the purging of genetically compromised cells from the brain, we would then expect that disruptions in this pathway would cause greater incorporation of cells into the adult brain as well as increased levels of DNA damage. Consistent with this idea, we observed increased numbers of calbindin^{+} Purkinje neurons in the brains of mice lacking either AIM2, Caspase-1/11, or Gasdermin-D (Fig. 3d, Extended Data Fig. 8). Furthermore, we also detected markedly enhanced staining of the DNA damage marker γH2AX in the brains of *Aim2*$^{-/-}$ mice (Fig. 3e–h). This increase in DNA damage was seen throughout the brain including in regions that have been linked to fear and anxiety, such as the amygdala (Fig. 3g–h). We also examined levels of DNA damage in the adult cortex using single-cell gel electrophoresis (‘comet assay’). These studies confirmed our previous γH2AX results and showed that deficits in AIM2 lead to substantially increased DNA damage accumulation as indicated by the higher comet tail moment in the brains of AIM2-deficient mice (Fig. 3i–j). Likewise, we also observed increased levels of γH2AX staining in brains of *Ice*$^{-/-}$ and *Gsdmd*$^{-/-}$ mice (Fig. 3k). Although the nature and timing of these dsDNA breaks remains to be determined, it is evident that deficits in AIM2 inflammasome signaling result in elevated accumulation of DNA damage in the brain. Collectively, these findings suggest that the AIM2 inflammasome and Gasdermin-D aid in the removal of DNA damage harboring cells from the brain.

CNS-derived inflammasomes shape behavior

Mounting evidence suggests that immune activation in the periphery can have profound effects on brain maturation and behavior[28]. Therefore, it is feasible that inflammasome signaling can shape behavior and neurodevelopment both through its local actions in the brain and also via its functions in the periphery. To investigate this in greater detail, we first sought to identify what CNS-derived cell types express *Aim2* during neurodevelopment. Using fluorescent in situ hybridization, we found that *Aim2* is appreciably expressed by microglia, astrocytes, and neurons in the developing brain (Extended Data Fig. 9a–b). Microglia are the innate immune sentinels of the brain and recent work suggests that microglia-coordinated innate immune responses can greatly impact brain development and function[29]. To our surprise, we found that deletion of Caspase-1 in CX3CR1-expressing cells, which includes microglia, does not result in the development of anxiety-related behaviors in either the open field or elevated plus maze tests (Extended Data Fig. 10a–c). In contrast, we found that conditional ablation of Caspase-1 from Nestin-expressing CNS cells (i.e. neurons, astrocytes, and oligodendrocyte lineage cells) in *Casp1*$^{fl/fl}$*Nestin*^{Cre} mice leads to anxiety-related behaviors and the accumulation of DNA damage in the brain (Fig. 4a–g).

These data indicate a specific role for Caspase-1 within the CNS in driving the observed behavioral phenotypes and preventing DNA damage accumulation.

Discussion

Our results underscore how deficits in the immune response to DNA insults can lead to impaired CNS development and neurological disease. The long-lived nature of neurons and glia, coupled with their exposure to high levels of replicative stress during neurodevelopment, makes the CNS especially vulnerable to DNA damage-induced dysfunction and pathology[18,30]. Yet, how the brain protects itself from genotoxic stress remains incompletely understood. Here we demonstrate that DNA damage surveillance by the AIM2 inflammasome is required for normal brain development and function. We found that the AIM2 inflammasome and downstream Gasdermin-D-mediated cell death contribute to the elimination of genetically compromised CNS cells. Furthermore, we report that disruptions in this pathway lead to the development of anxiety-related behaviors, DNA damage accumulation in the CNS, and increased numbers of neurons in the adult brain (Extended Data Fig. 10d). It is commonly assumed that CNS dieback relies solely on apoptosis as a cell death pathway to remove unwanted cells. Yet, this assumption was made at a time when it was thought that there were only two forms of cell death (i.e. apoptosis and necrosis). Our findings demonstrating decreased CNS cell pruning and greater incorporation of neurons into the brains of Gasdermin-D-deficient mice implicate the involvement of another form of cell death, namely pyroptosis, in the sculpting of the brain. Further elucidation of the functional consequence of DNA damage sensing by the innate immune system may offer novel strategies to treat a wide range of neurological disorders that are perpetuated by genotoxic stress.

Methods

Mice

All mouse experiments were performed in accordance with the relevant guidelines and regulations of the University of Virginia and approved by the University of Virginia Animal Care and Use Committee. Wild-type (WT) C57BL/6, *Aim2*$^{-/-}$[3], *Casp1/11*$^{-/-}$ (*Ice*$^{-/-}$)[31], *Nlrp3*$^{-/-}$[32], *Myd88*$^{-/-}$[33], *Il1r*$^{-/-}$[34], *Il18r*$^{-/-}$[35], R26-CAG-ASC-citrine[15], *Casp11*$^{-/-}$[36], *Casp1*$^{fl/fl}$[37], *Nestin*^{Cre}[38], and *Cx3cr1*^{Cre}[39] mice were obtained from The Jackson Laboratory. *Gsdmd*$^{-/-}$ mice were generously provided by Vishva Dixit[26]. Mice were housed and behavior was conducted in specific pathogen-free conditions under standard 12 h light/dark cycle conditions in rooms equipped with control for temperature (21 ± 1.5°C) and humidity (50 ± 10%).

Immunocytochemistry

Immunofluorescence: Adult male mice were perfused with 4% paraformaldehyde in PBS. The brains were removed and fixed in 4% paraformaldehyde in phosphate buffered saline (PBS) overnight at 4 °C. After dehydration in 30% sucrose, 30 μm sagittal sections were obtained using a Leica CM1950 cryostat (Leica). Sections were permeabilized with blocking solution containing 0.4% Triton X-100, 2% donkey serum, and 1% bovine serum

albumin (BSA) in PBS for 1 h at room temperature and then incubated with primary antibodies overnight at 4°C. Primary antibodies were diluted as follows: anti-GFAP (Invitrogen, 13–0300, 1:500), anti-calbindin (Sigma, C9848, 1:1,000), anti-γH2AX (abcam, ab11174, 1:1,000), anti-53bp1 (abcam, ab21083, 1:1,000). The following day, sections were incubated with fluorescently conjugated secondary antibodies (Invitrogen) for 2 hrs at room temperature, and mounted in ProLong Gold antifade reagent (Invitrogen). Images of stained brain sections were acquired using a confocal microscope (Leica TCS SP8) and analyzed using ImageJ software. ASC visualization was accomplished using 488 nm detectors. 2–3 sections from each individual mouse were analyzed and averages were used for data analysis.

TUNEL Assay

Cell death was measured *in vivo* using a TUNEL assay (Roche, 11 684 795 910) according to manufacturer's instructions. Briefly, p5 brains were perfused with PBS followed by 4% PFA and then drop fixed in 4% PFA for 24 hrs. After dehydration in 30% sucrose, 30 μm sagittal sections were obtained using a Leica CM1950 cryostat (Leica). Sections were permeabilized with blocking solution containing 0.4% Triton X-100, 2% donkey serum, and 1% bovine serum albumin (BSA) in PBS for 1 h at room temperature and then incubated with primary antibodies overnight at 4°C and secondary antibodies for 2 hrs at room temp. Sections were mounted and allowed to dry on a slide before 50 μL of the TUNEL reaction mixture was added to each section. Slides were then incubated in a humidified atmosphere for 60 min at +37°C in the dark. Slides were then rinsed 3x with 1x PBS and then analyzed under a fluorescence microscope using a 488nm laser. 2–3 sections from each individual mouse were analyzed and averages were used for data analysis.

Comet Assay

The comet assay was performed using the Oxiselect Comet Assay Kit (Cell-Biolabs Inc.) according to the manufacturer's instructions with minor modifications. Slides were coated in low melting agarose the night before the assay and left to dry overnight. Cells were added to the top of agarose-coated slides followed by immediate placement of a cover slip to ensure an even and flat distribution of cells on the slide.

Mixed Neuron/Glia Culture

Mixed CNS culture was performed according to a previously established protocol with minor modifications[40]. All cell culture plates were pre-coated with Poly-D-Lysine before seeding. P0 pups were euthanized and the brain was placed into cold Neuron-Glia dissection buffer. After removal of the meninges, the cortex was detached and placed in a 50 mL conical with cold Neuron-Glia dissection buffer. The cortices were triturated into a single cell suspension using serological pipette and 3×10^5 cells were plated per well in a 24-well plate. Cells were cultured for 10–14 days before treatment, with media changes every 2–3 days.

dsDNA Stimulations

After 10–14 days in culture, cells were stimulated +/− lipopolysaccharide (LPS) (0.5 μg/mL) in stimulation media containing Iscove's Modified Dulbecco's Medium (Gibco), 1% Penicillin/Strepomycin, 10% fetal bovine serum, 1% L-Glutamine, and 50 μM 2-beta-mercaptoethanol for 4 hrs at 37°C. After 4 hrs, cells were given additional stimuli to induce/mimic dsDNA breaks.

***Etoposide* (abcam, ab120227):** A 100 mM stock was prepared in DMSO according to the manufacturer's instructions and diluted to a final concentration of 20 μM or 100 μM in stimulation media. Cells were treated with +/− etoposide and incubated overnight at 37°C and supernatants were collected the following morning for additional assays.

Ionizing Radiation: Cells were exposed to 40 Gy for 20 min and incubated overnight at 37°C. Supernatants were collected the following morning for additional assays.

P5 mice were exposed to 14 Gy ionizing radiation and then returned to their home cage for 6 hrs. After 6 hrs, brain tissue was harvested for immunofluorescence and TUNEL staining.

PolydA:dT: Mixed glia cells were transfected with +/− *polydA:dT* using lipofectamine 2000 reagent (Invitrogen, 11668–030) according to the manufacturer's instructions and incubated overnight at 37°C. Supernatants were collected the following morning for additional assays.

Cytotoxicity

LDH release was measured using the CytoTox96 Non-Radioactive Cytotoxicity Assay (Promega, G1780) according to the manufacturer's instructions. Maximum LDH release control for each plate was generated using Lysis Solution.

RNA *in situ* Hybridization (ISH)

Brains from p5 pups were formalin fixed for 48 hrs, embedded in paraffin, and cut into 5 μm sections. In situ hybridization was carried out according to the manufacturer's instructions (Affymetrix, QVT0012). Probes recognizing *Aim2* RNA (NM_001013779) were multiplexed with probes recognizing RNA expressed in neurons (*Rbfox3*, NM_001039167), microglia (*Aif1*, NM_019467), and astrocytes (*Gfap*, NM_010277). Ubiquitin (*Ubc*, NM_019639) was used as a positive control.

Behavioral Testing

All behavioral testing was performed according to previously established behavioral methodologies. Behavioral experiments were carried out during daylight hours in a blinded fashion. All behavior was carried out using adult male mice (8–12 weeks old).

Elevated Plus Maze

Anxiety was assessed using an elevated plus maze. The elevated plus maze was comprised of two open arms (35 × 6 cm^2) and two closed arms (35 × 6 cm^2) with black plexiglass walls (20 cm in height) that extended from a common central platform (8 × 6 cm^2). The apparatus

was constructed from polypropylene and Plexiglas (white floor, black walls) and elevated to a height of (121 cm) above floor level. Mice were individually placed on the center square, facing an open arm, and allowed to freely explore the apparatus for 5 min. Activity was measured by a computer-assisted TopScan optical animal activity system (version 3.0).

Open Field Testing

Spontaneous locomotor activity and anxiety was assessed in an open field test. The open field consists of a square arena (40 × 40 cm^2) with white Plexiglas walls and floor, evenly illuminated. All mice were individually placed in the upper left corner of the open field and left undisturbed to explore the arena over a 10 min session. Activity was measured by a computer-assisted TopScan optical animal activity system (version 3.0). Bouts into and time spent in a central square (15 × 15 cm^2) of the open field were automatically recorded as center bouts and center time, respectively. After the 10 min open field exploration, mice were returned to their home cage and number of urine stains and fecal pellets in the field were counted.

Sucrose Preference

Depression-associated behaviors were assessed by measuring sucrose preference. Mice were given access to both untreated water and 2% sucrose water for 3 days. To prevent possible effects of side-preference in drinking behavior, the position of the bottles in the cage was alternated every other day. No previous food or water deprivation was applied before the test.

Escape Behavior

Modified tail suspension test was used to measure escape behavior. Mice were raised by their tail 30 cm into the air and assessed for escape behavior. Mice were monitored until they became immobile.

Visual Platform Test

Visual performance was assessed using a visual platform in the Morris Water Maze. Mice were placed in clear water with a visible white platform and performance was evaluated as time spent reaching the platform.

Statistics and reproducibility

All statistical analyses were performed using GraphPad Prism. Statistical significance was calculated by unpaired two-tailed Student's *t*-test, one-way analysis of variance (ANOVA) with Tukey's post hoc tests or two-way ANOVA with Tukey's post hoc tests. *P*-values <0.05 were considered significant. Sample size was chosen on the basis of similar previous studies[5,25], and not on statistical methods to predetermine sample size. All mouse experiments and data quantification were done in a blinded and randomized fashion.

Data Availability

Source Data for Figs. 1–4 and Extended Data Figs. 1, 3–7, and 9–10 containing raw data for all experiments, are provided with the paper. All other data are available from the corresponding author upon request.

Extended Data

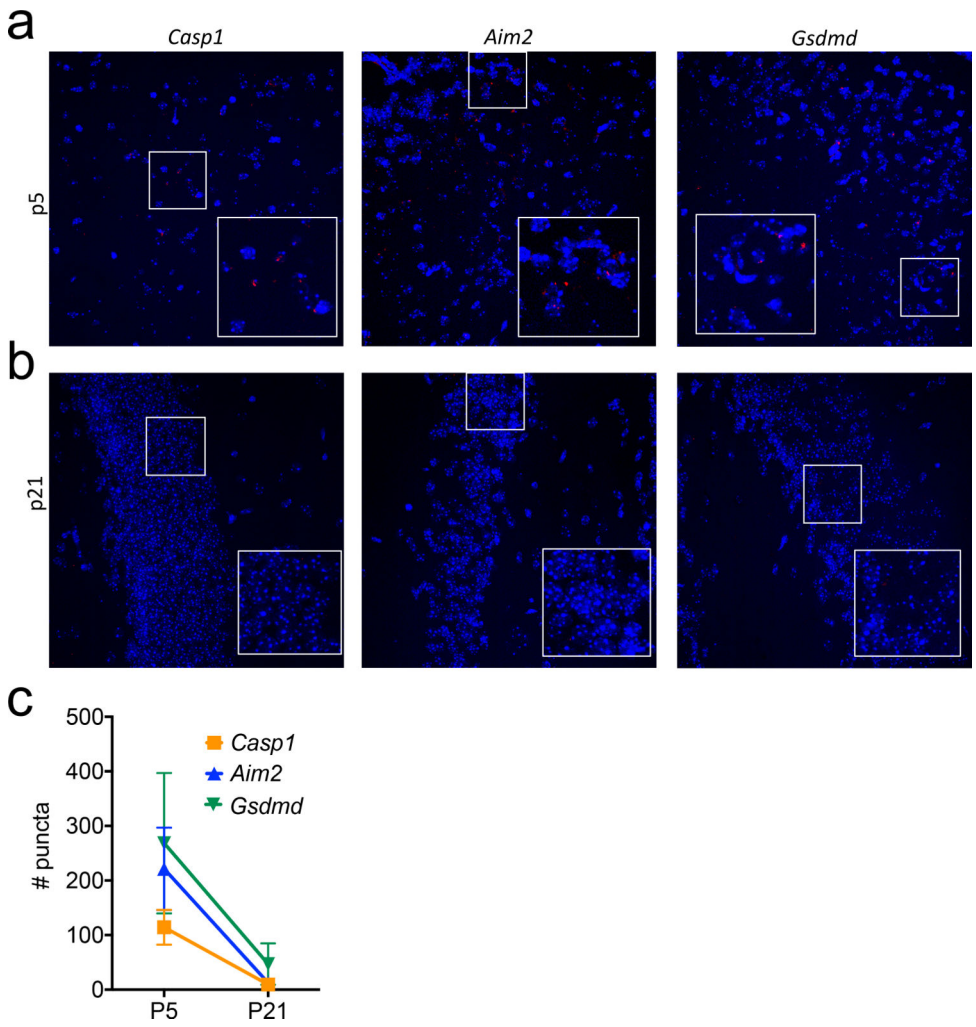

Extended Data Figure 1. Molecular components of the AIM2 inflammasome are abundantly expressed in the brain during neurodevelopment.

(a-c) Brains from (a) p5 and (b) p21 WT mice were evaluated for the mRNA expression of inflammasome component genes (red) *Casp1* (p5 *n*=4, p21 *n*=2), *Aim2* (p5 *n*=3, p21 *n*=2), and *Gsdmd* (p5 *n*=3, p21 *n*=2) using RNA scope. (c) Quantification of *Casp1* (p5 *n*=4, p21 *n*=2), *Aim2* (p5 *n*=3, p21 *n*=2), and *Gsdmd* (p5 *n*=3, p21 *n*=2) mRNA puncta in the hippocampus per 40X image; from 1 experiment. Error bars depict mean ± s.e.m. *n* values refer to biological replicates.

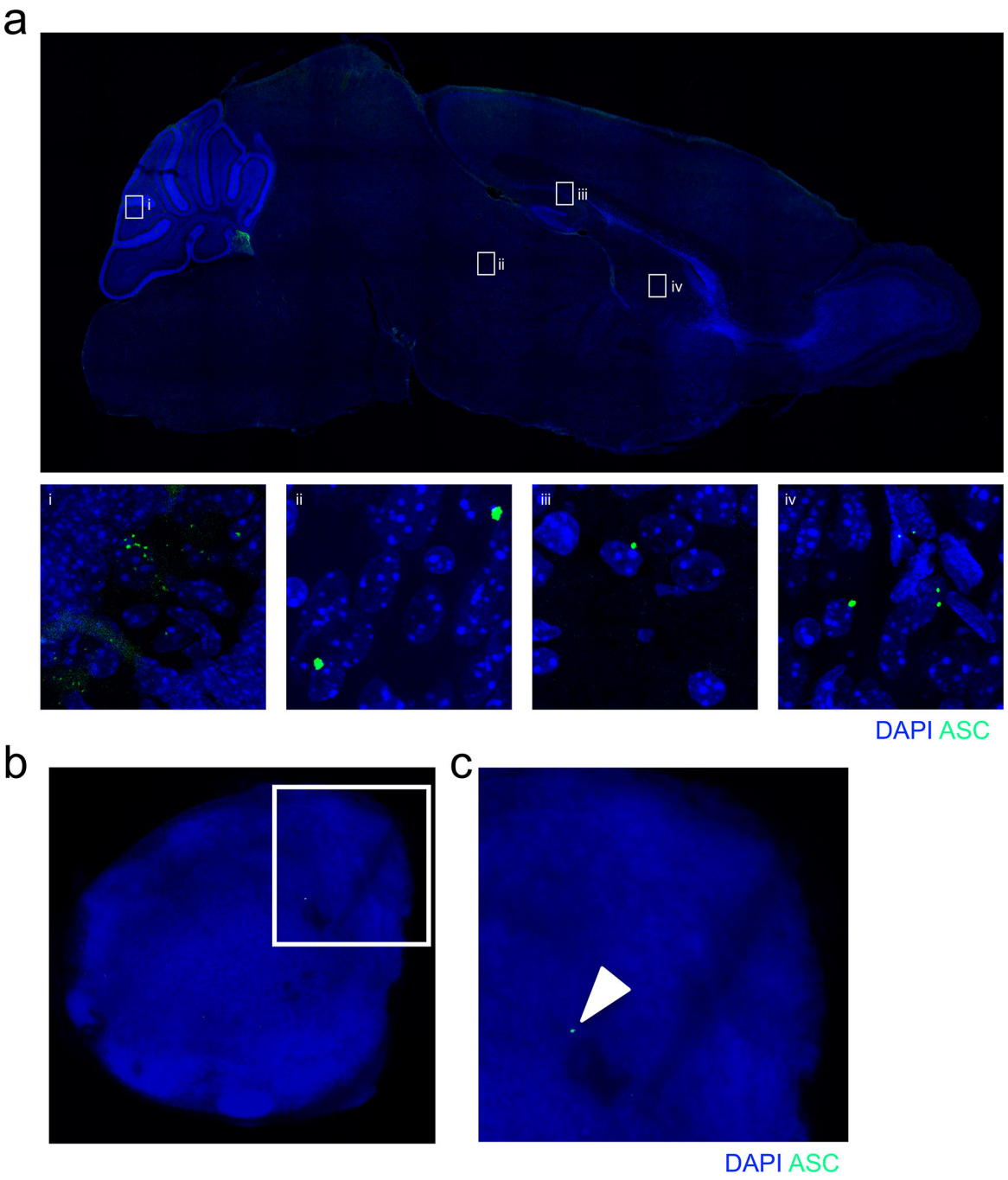

Extended Data Figure 2. ASC speck formation routinely occurs in the developing brain but is rare in mature lymph nodes under steady-state conditions.

(a) 10X sagittal image of ASC speck formation (green) in the brain of p5 ASC-Citrine reporter mice. ASC specks are detected throughout the brain using a 40X objective including in the (i) cerebellum, (ii) midbrain, (iii) hippocampus, and (iv) thalamus. Representative images from 3 independent experiments with similar results. (b-c) Adult (8–12 weeks old) ASC-citrine reporter mice were evaluated for peripheral inflammasome activation based on (b) ASC speck formation (green) in the deep cervical lymph node (DCLN) using confocal microscopy with a 10X objective. (c) Arrow shows zoomed in image of ASC speck (green)

formed in DCLN. Representative images from 2 independent experiments with similar results.

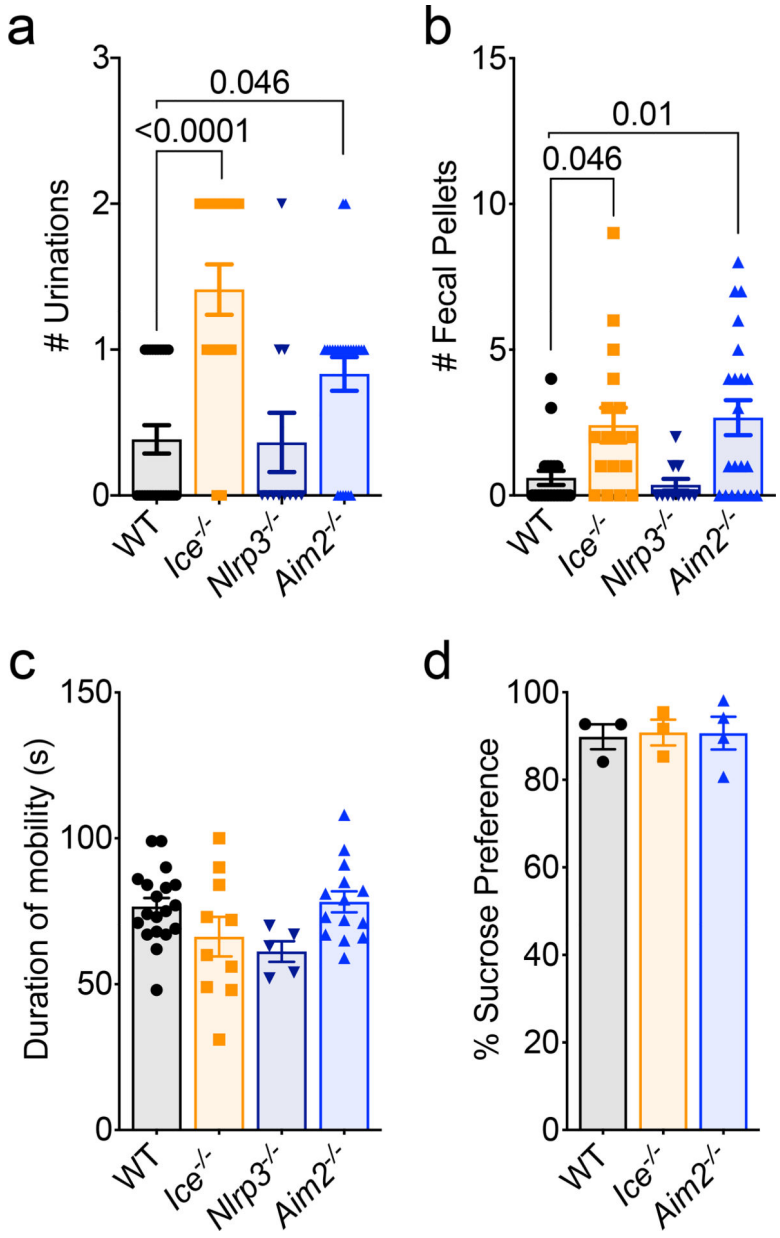

Extended Data Figure 3. Lack of AIM2 inflammasome signaling results in an increase in anxiety-related behaviors but not depressive-related behaviors.

Adult (8–12 weeks old) WT, *Ice*$^{-/-}$, *Aim2*$^{-/-}$, and *Nlrp3*$^{-/-}$ mice were assessed for behavioral abnormalities. (a) Number of urinations (WT n=26, *Ice*$^{-/-}$ n=17, *Nlrp3*$^{-/-}$ n=11, *Aim2*$^{-/-}$ n=24; from 3 independent experiments) and (b) number of fecal pellets (WT n=20, *Ice*$^{-/-}$ n=17, *Nlrp3*$^{-/-}$ n=11, *Aim2*$^{-/-}$ n=21; from 3 independent experiments) were measured during 10 minutes of open field-testing. Depressive behaviors were evaluated in adult male mice using the (c) tail suspension test for escape behavior (WT n=19, *Ice*$^{-/-}$ n=10, *Nlrp3*$^{-/-}$ n=5, *Aim2*$^{-/-}$ n=14; from 2 independent experiments) and (d) sucrose

preference test (WT n=3, *Ice*$^{-/-}$ n=3, *Aim2*$^{-/-}$ n=4; from 1 independent experiment). All n values refer to the number of mice used. Error bars depict mean ± s.e.m. Statistics calculated by one-way ANOVA with Tukey's post hoc tests.

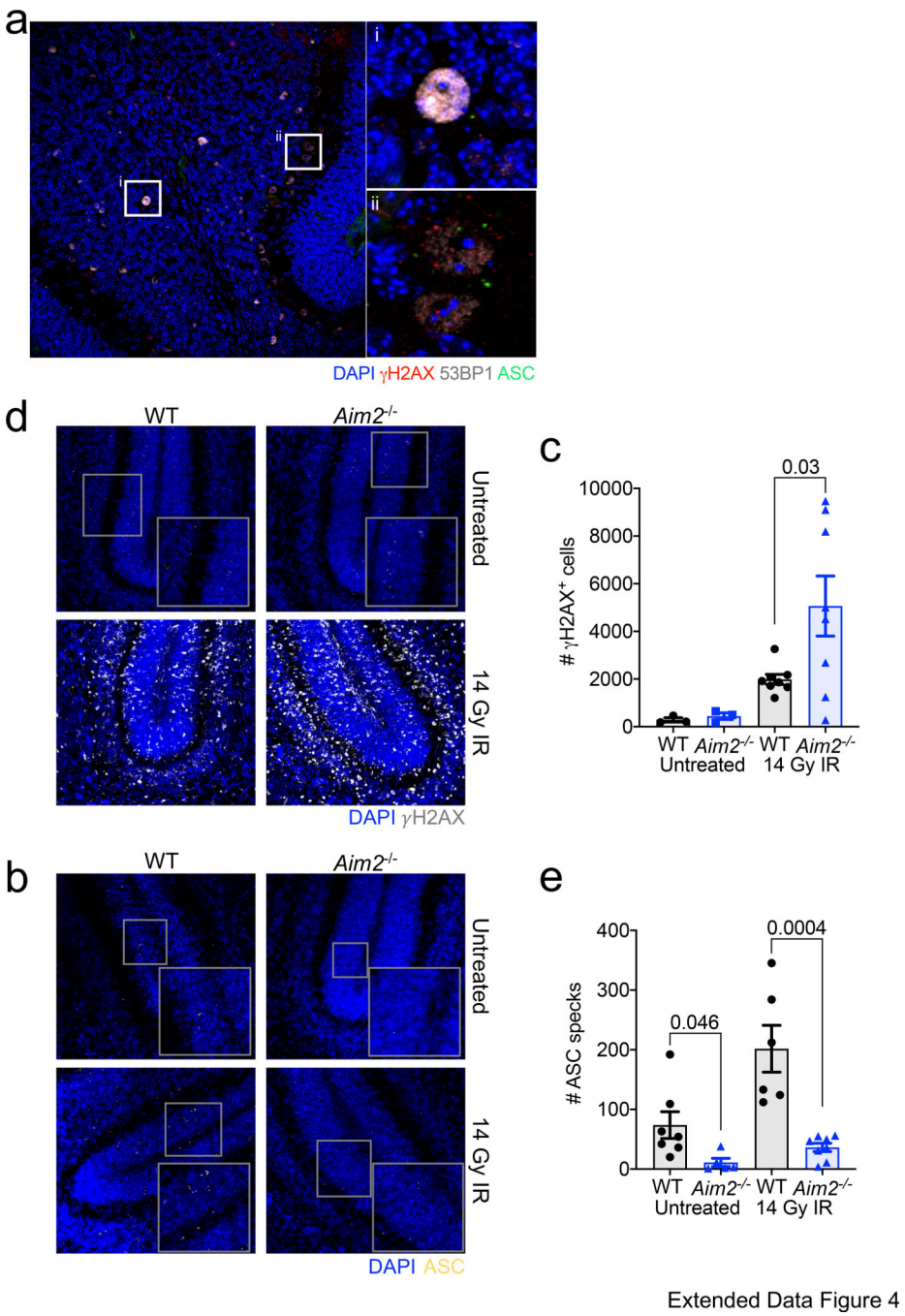

Extended Data Figure 4

Extended Data Figure 4. ASC specks form in response to DNA damage in the developing brain.

(a) Brains from p5 WT mice were evaluated for localization of ASC specks (green) in relation to DAPI^{+} nuclei (blue) harboring DNA damage (γH2AX (red), 53BP1 (grey)) in the cerebellum. (i, ii) Zoomed in regions of 40X images showing ASC specks formed in close

proximity to nuclei harboring DNA damage. Representative images from 4 mice with similar results from 1 experiment. Differences in nuclei size likely reflect specific stages in replication, DNA repair, differentiation, or cell death the individual cells are in as well as differences seen across CNS cell types. (b-e) Postnatal day 5 (p5) WT and *Aim2*$^{-/-}$ mice received either control treatment or 14 Grays (14 Gy) of ionizing radiation (IR) to induce DNA damage. Brains were harvested 6 hrs later and then immunostaining was conducted to measure DNA damage induction (γH2AX staining) and inflammasome activation (ASC speck formation) in the cerebellum. (b) Representative 20X cerebellar images of γH2AX staining; from 2 independent experiments with similar results. (c) Quantification of γH2AX staining in the cerebellum (Untreated: WT *n*=3, *Aim2*$^{-/-}$ *n*=3; IR treated: WT *n*=8, *Aim2*$^{-/-}$ *n*=8; from 2 independent experiments). (d) Representative 20X cerebellar images of ASC speck formation; from 2 independent experiments with similar results. (e) Quantification of ASC speck formation in the cerebellum (Untreated: WT *n*=7, *Aim2*$^{-/-}$ *n*=5; IR treated: WT *n*=6, *Aim2*$^{-/-}$ *n*=8; from 2 independent experiments). All *n* values refer to the number of mice used. Error bars depict mean ± s.e.m. Statistics calculated by unpaired two-tailed Student's *t*-test.

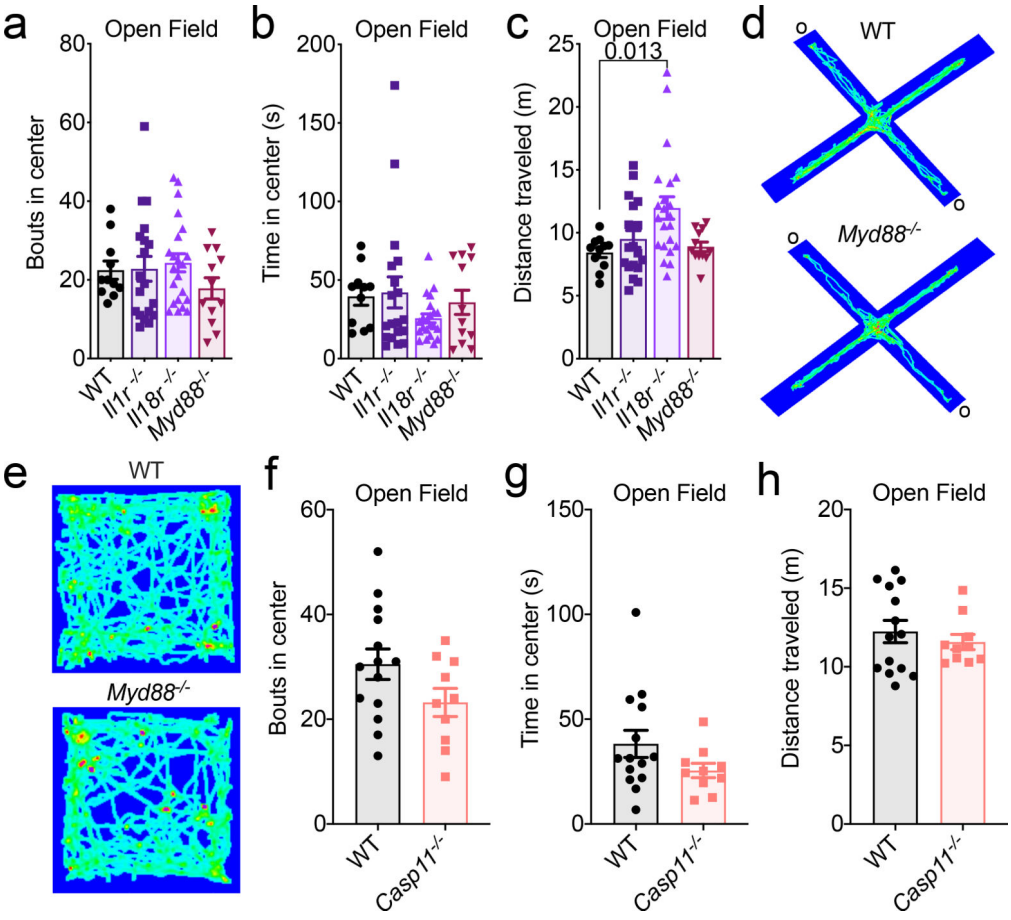

Extended Data Figure 5. Anxiety phenotypes do not develop in mice that lack IL-1R, IL-18R, MYD88, or Caspase-11.

All behavioral testing was conducted on adult (8–12 weeks old) mice. (a-c) Behaviors for anxiety were evaluated by (a) bouts into and (b) time spent in the center of the open field arena with (c) total distance traveled (WT n=11, *Il1r*$^{-/-}$ n=19, *Il18r*$^{-/-}$ n=22, *Myd88*$^{-/-}$ n=12; from 3 independent experiments). (d) Anxiety-related behaviors were assessed in WT and *Myd88*$^{-/-}$ mice using the elevated plus maze. Representative heat maps from 4 independent experiments with similar results depicting path of travel through open arms (o) and closed arms of the maze. (e) Representative heat maps from 4 independent experiments with similar results of the path traveled by adult WT and *Myd88*$^{-/-}$ mice in the open field arena. (f-h) Quantification of (f) bouts into and (g) time in center of the open field arena with (h) distance traveled (WT n=14, *Casp11*$^{-/-}$ n=10; from 2 independent experiments). All n values refer to the number of mice used. Error bars depict mean ± s.e.m. Statistical analysis by (a-c) one-way ANOVA with Tukey's post hoc tests or (f-h) unpaired two-tailed Student's t-test showed no statistically significant differences.

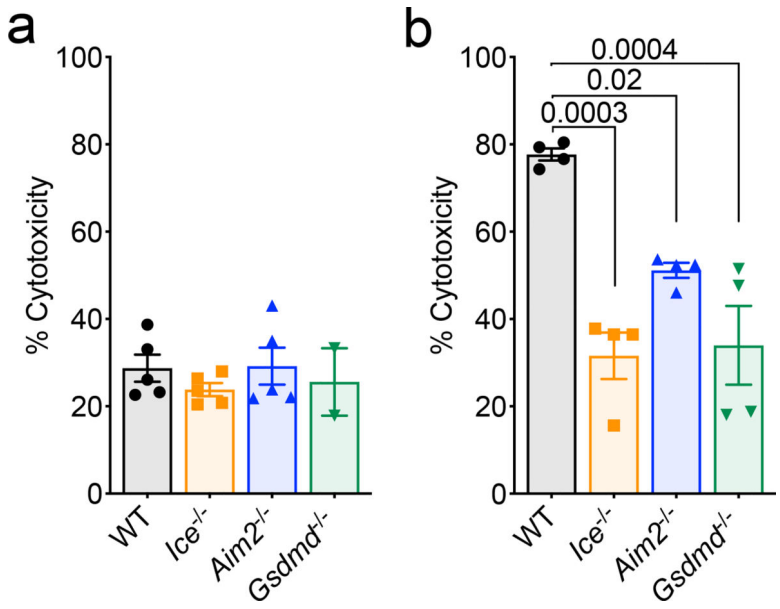

Extended Data Figure 6. Genetic ablation of the AIM2 inflammasome or Gasdermin-D in CNS cells limits cell death in response to DNA insults.

Mixed neural cultures were generated from postnatal day 0 (p0) WT, *Ice*$^{-/-}$, *Aim2*$^{-/-}$, and *Gsdmd*$^{-/-}$ mice. (a) Mixed neural cell cultures were left untreated to test for baseline differences in cytotoxicity (WT n=5, *Ice*$^{-/-}$ n=5, *Aim2*$^{-/-}$ n=5, and *Gsdmd*$^{-/-}$ n=2). (b) Mixed neural cell cultures were primed with LPS for 4 hrs followed by transfection with PolydA:dT (WT n=4, *Ice*$^{-/-}$ n=4, *Aim2*$^{-/-}$ n=4, and *Gsdmd*$^{-/-}$ n=4). Cell death was measured by LDH release after overnight stimulation. Representative data from 3 independent experiments. All n values refer to biological replicates from one representative experiment. Error bars depict mean ± s.e.m. Statistics calculated by one-way ANOVA with Tukey's post hoc tests.

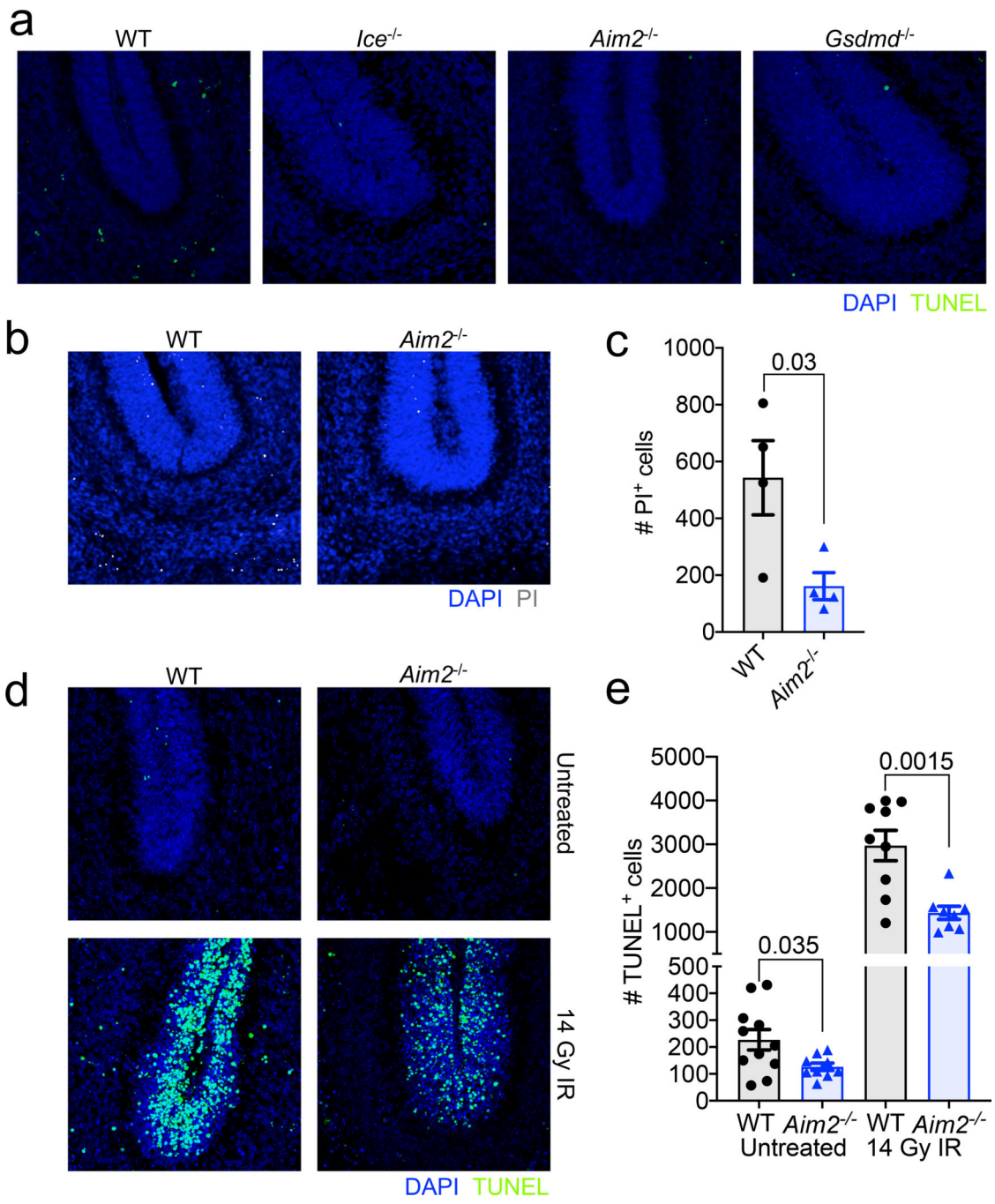

Extended Data Figure 7. AIM2 contributes to CNS cell death during neurodevelopment and in response to ionizing radiation.

(a) Representative 20X images from p5 WT, *Ice*$^{-/-}$, *Aim2*$^{-/-}$, and *Gsdmd*$^{-/-}$ mice showing TUNEL^{+} cells (green) in the cerebellum. Images are representative from 2 independent experiments with similar results. (b) Representative images of additional markers of cell death (propidium iodide (PI), grey) in p5 WT and *Aim2*$^{-/-}$ mice. (c) Quantification of PI^{+} cells in the cerebellum of p5 WT n=4 and *Aim2*$^{-/-}$ n=4 mice; from 1 independent experiment. (d-e) p5 WT and *Aim2*$^{-/-}$ mice received either control treatment or 14 Grays (14 Gy) of ionizing radiation (IR) to induce DNA damage. Brains were harvested 6 hrs later

and then TUNEL assay staining was conducted on cerebellar sections to evaluate cell death. (d) Representative 20X images showing TUNEL staining in the cerebellum of untreated and irradiated p5 WT and *Aim2*$^{-/-}$ mice; from 3 independent experiments with similar results. (e) Quantification of number of TUNEL^{+} cells in the cerebellums of untreated and irradiated WT (n=11 untreated; n=9 IR) and *Aim2*$^{-/-}$ (n=9 untreated; n=8 IR) mice; from 3 independent experiments. All n values refer to the number of mice used. Error bars depict mean ± s.e.m. Statistics calculated by unpaired two-tailed Student's t-test.

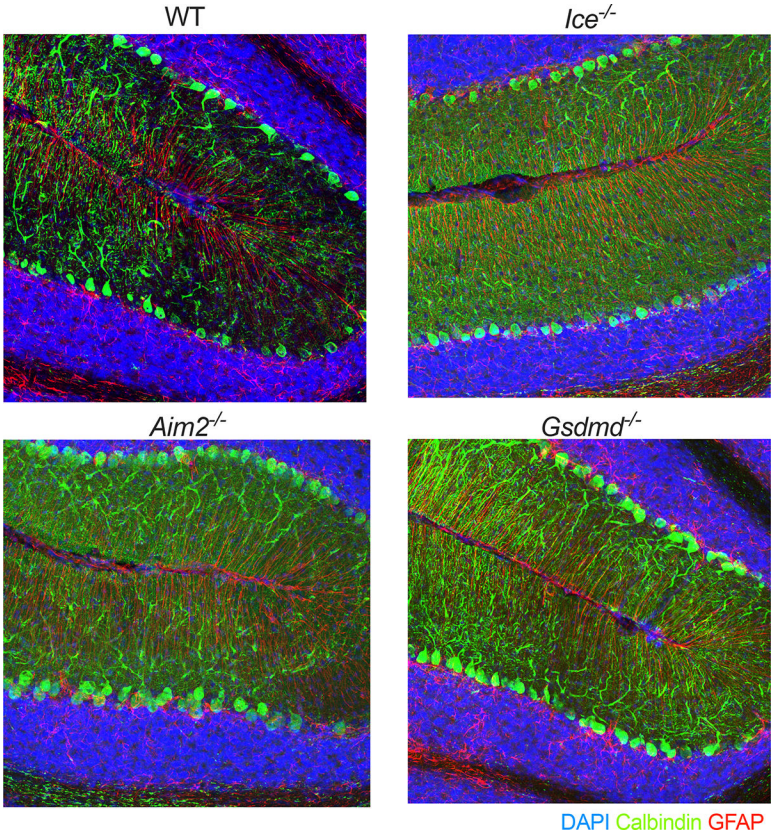

Extended Data Figure 8. Lack of AIM2 inflammasome components increases the number of Purkinje neurons that are incorporated into the adult brain.

Representative 20X images of cerebellums from adult (8–12 weeks old) WT, *Ice*$^{-/-}$, *Aim2*$^{-/-}$, and *Gsdmd*$^{-/-}$ mice showing an increase in number of Purkinje cells (calbindin^{+} cells) in mice lacking inflammasome components. Representative images from 3 independent experiments with similar results.

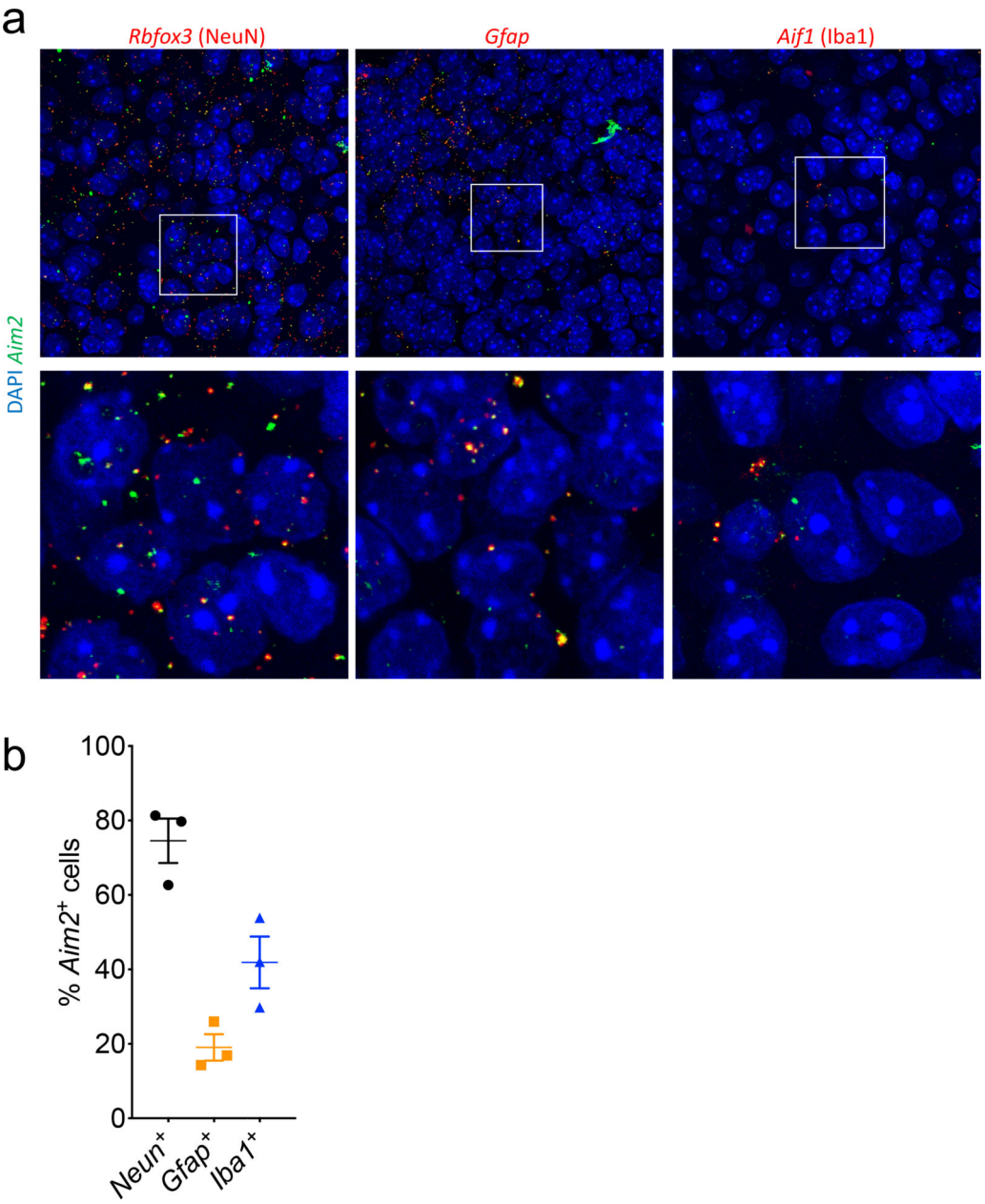

Extended Data Figure 9. *Aim2* is expressed by neurons, astrocytes, and microglia in the developing brain.

Brains from p5 WT mice (n=3; from 1 experiment) were evaluated for expression of *Aim2* using RNA scope. (a) Images showing co-expression of *Aim2* (green) and CNS cell-specific genes *Rbfox3*: NeuN (red), *Gfap*: GFAP (red), and *Aif1*: Iba1 (red) in the hippocampus. (b) Quantification showing percentage of CNS cells in 40X images that are positive for *Aim2.* Error bars depict mean ± s.e.m. n values refer to biological replicates.

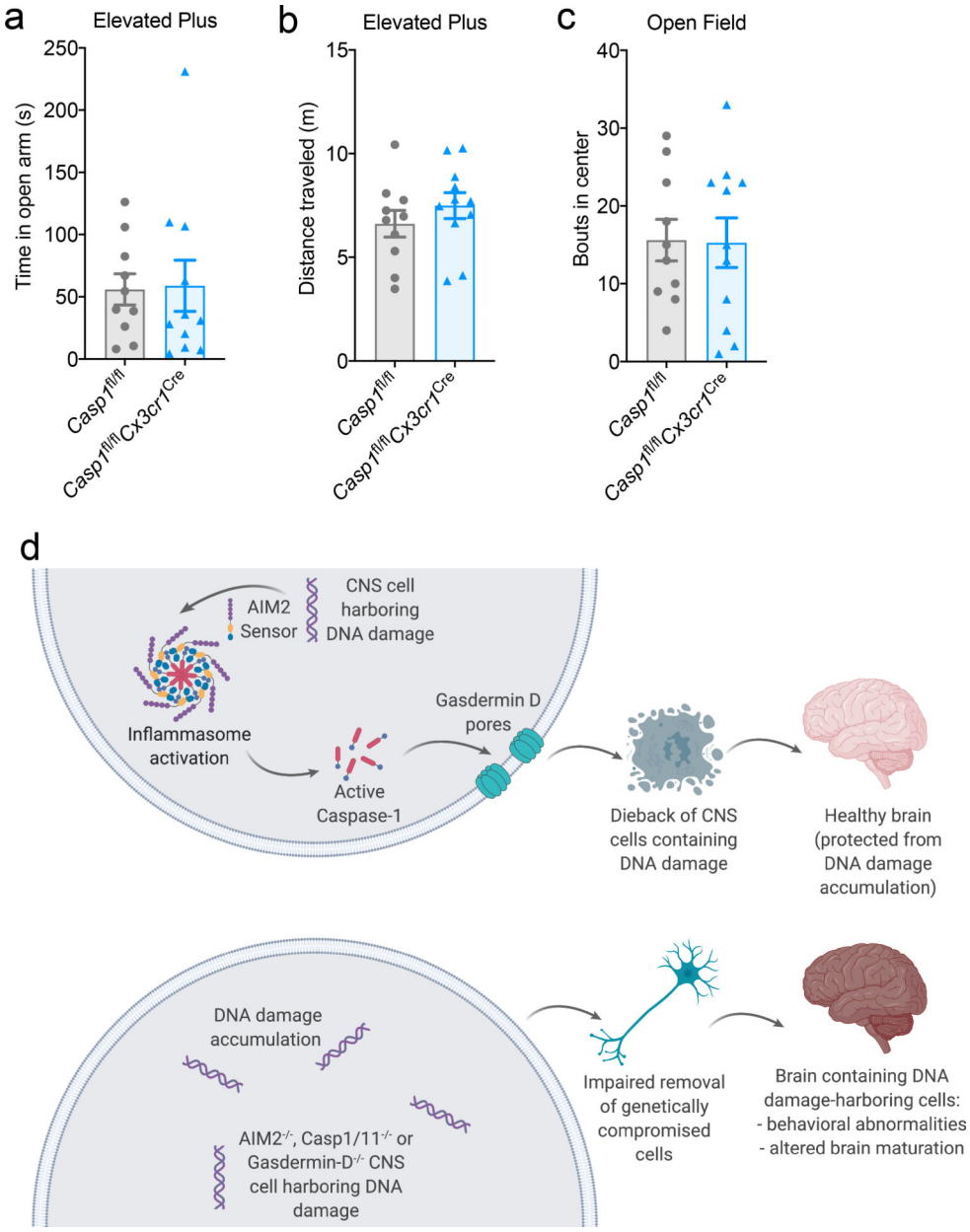

Extended Data Figure 10. Deletion of Caspase-1 in CX3CR1-expressing cells does not result in the development of anxiety-related behaviors.

Adult (8–12 weeks old) *Casp1*$^{fl/fl}$ *n*=10 and *Casp1*$^{fl/fl}$*Cx3cr1*^{Cre} *n*=11 mice were evaluated for anxiety-related behaviors using (a) time in open arms and (b) distance traveled in the elevated plus maze along with (c) total bouts into the center of the open field arena; from 2 independent experiments. All *n* values refer to the number of mice used. (d) Schematic of the proposed role that DNA damage surveillance by the AIM2 inflammasome plays in neurodevelopment. Error bars depict mean ± s.e.m. Statistical analysis by unpaired two-tailed Student's *t*-test showed no statistically significant differences.

Supplementary Material

Refer to Web version on PubMed Central for supplementary material.

Acknowledgements

We thank members of the Lukens lab and the Center for Brain Immunology and Glia (BIG) for valuable discussions. This work was supported by The Hartwell Foundation (Individual Biomedical Research Award to J.R.L.), a Rettsyndrome.org grant (22349 to J.R.L.), The Owens Family Foundation (awarded to J.R.L.), and a NARSAD Young Investigator Grant from the Brain & Behavior Research Foundation (27515 to J.R.L.). C.R.L was supported by a NIH National Institute of General Medical Sciences predoctoral training grant (3T32GM008328) and a Wagner Fellowship. A.C.B. was supported by a Medical Scientist Training Program Grant (5T32GM007267-38) and an Immunology Training Grant (5T32AI007496-25). H.E.E was supported by a Cell and Molecular Biology Training Grant (T32GM008136). E.L.F. was supported by a National Multiple Sclerosis Foundation Postdoctoral Fellowship (FG-1707-28590). C.E.B. was supported by Hutcheson and Stull Undergraduate Research Fellowships.

Abbreviations:

AIM2	absent in melanoma 2
ASC	apoptosis-associated speck-like protein containing CARD
CNS	central nervous system
dsDNA	double-stranded DNA
IL	interleukin
MWM	Morris water maze
NLRP3	Nucleotide-binding oligomerization domain (NOD)-like receptor Family Pyrin Domain Containing 3

References

1. Fernandes-Alnemri T, Yu JW, Datta P, Wu J & Alnemri ES AIM2 activates the inflammasome and cell death in response to cytoplasmic DNA. Nature 458, 509–513, doi:10.1038/nature07710 (2009). [PubMed: 19158676]
2. Hornung V et al. AIM2 recognizes cytosolic dsDNA and forms a caspase-1-activating inflammasome with ASC. Nature 458, 514–518, doi:10.1038/nature07725 (2009). [PubMed: 19158675]
3. Rathinam VA et al. The AIM2 inflammasome is essential for host defense against cytosolic bacteria and DNA viruses. Nat Immunol 11, 395–402, doi:10.1038/ni.1864 (2010). [PubMed: 20351692]
4. Guo H, Callaway JB & Ting JP Inflammasomes: mechanism of action, role in disease, and therapeutics. Nat Med 21, 677–687, doi:10.1038/nm.3893 (2015). [PubMed: 26121197]
5. Choi GB et al. The maternal interleukin-17a pathway in mice promotes autism-like phenotypes in offspring. Science 351, 933–939, doi:10.1126/science.aad0314 (2016). [PubMed: 26822608]
6. Allan SM, Tyrrell PJ & Rothwell NJ Interleukin-1 and neuronal injury. Nat Rev Immunol 5, 629–640, doi:10.1038/nri1664 (2005). [PubMed: 16034365]
7. Felderhoff-Mueser U, Schmidt OI, Oberholzer A, Buhrer C & Stahel PF IL-18: a key player in neuroinflammation and neurodegeneration? Trends Neurosci 28, 487–493, doi:10.1016/j.tins.2005.06.008 (2005). [PubMed: 16023742]

8. Dantzer R, O'Connor JC, Freund GG, Johnson RW & Kelley KW From inflammation to sickness and depression: when the immune system subjugates the brain. Nat Rev Neurosci 9, 46–56, doi:10.1038/nrn2297 (2008). [PubMed: 18073775]
9. Garber C et al. Astrocytes decrease adult neurogenesis during virus-induced memory dysfunction via IL-1. Nat Immunol 19, 151–161, doi:10.1038/s41590-017-0021-y (2018). [PubMed: 29292385]
10. Walsh JG, Muruve DA & Power C Inflammasomes in the CNS. Nat Rev Neurosci 15, 84–97, doi:10.1038/nrn3638 (2014). [PubMed: 24399084]
11. Yamaguchi Y & Miura M Programmed cell death in neurodevelopment. Dev Cell 32, 478–490, doi:10.1016/j.devcel.2015.01.019 (2015). [PubMed: 25710534]
12. Kuan CY et al. The Jnk1 and Jnk2 protein kinases are required for regional specific apoptosis during early brain development. Neuron 22, 667–676 (1999). [PubMed: 10230788]
13. Cecconi F, Alvarez-Bolado G, Meyer BI, Roth KA & Gruss P Apaf1 (CED-4 homolog) regulates programmed cell death in mammalian development. Cell 94, 727–737 (1998). [PubMed: 9753320]
14. Yoshida H et al. Apaf1 is required for mitochondrial pathways of apoptosis and brain development. Cell 94, 739–750 (1998). [PubMed: 9753321]
15. Tzeng TC et al. A Fluorescent Reporter Mouse for Inflammasome Assembly Demonstrates an Important Role for Cell-Bound and Free ASC Specks during In Vivo Infection. Cell Rep 16, 571–582, doi:10.1016/j.celrep.2016.06.011 (2016). [PubMed: 27346360]
16. Herzog KH, Chong MJ, Kapsetaki M, Morgan JI & McKinnon PJ Requirement for Atm in ionizing radiation-induced cell death in the developing central nervous system. Science 280, 1089–1091 (1998). [PubMed: 9582124]
17. Takashima H et al. Mutation of TDP1, encoding a topoisomerase I-dependent DNA damage repair enzyme, in spinocerebellar ataxia with axonal neuropathy. Nat Genet 32, 267–272, doi:10.1038/ng987 (2002). [PubMed: 12244316]
18. McKinnon PJ Maintaining genome stability in the nervous system. Nat Neurosci 16, 1523–1529, doi:10.1038/nn.3537 (2013). [PubMed: 24165679]
19. McKinnon PJ Genome integrity and disease prevention in the nervous system. Genes Dev 31, 1180–1194, doi:10.1101/gad.301325.117 (2017). [PubMed: 28765160]
20. Schumacher B, Garinis GA & Hoeijmakers JH Age to survive: DNA damage and aging. Trends Genet 24, 77–85, doi:10.1016/j.tig.2007.11.004 (2008). [PubMed: 18192065]
21. Hoeijmakers JH DNA damage, aging, and cancer. N Engl J Med 361, 1475–1485, doi:10.1056/NEJMra0804615 (2009). [PubMed: 19812404]
22. Hu B et al. The DNA-sensing AIM2 inflammasome controls radiation-induced cell death and tissue injury. Science 354, 765–768, doi:10.1126/science.aaf7532 (2016). [PubMed: 27846608]
23. Denes A et al. AIM2 and NLRC4 inflammasomes contribute with ASC to acute brain injury independently of NLRP3. Proc Natl Acad Sci U S A 112, 4050–4055, doi:10.1073/pnas.1419090112 (2015). [PubMed: 25775556]
24. Adamczak SE et al. Pyroptotic neuronal cell death mediated by the AIM2 inflammasome. J Cereb Blood Flow Metab 34, 621–629, doi:10.1038/jcbfm.2013.236 (2014). [PubMed: 24398937]
25. Wu PJ, Liu HY, Huang TN & Hsueh YP AIM 2 inflammasomes regulate neuronal morphology and influence anxiety and memory in mice. Sci Rep 6, 32405, doi:10.1038/srep32405 (2016). [PubMed: 27561456]
26. Kayagaki N et al. Caspase-11 cleaves gasdermin D for non-canonical inflammasome signalling. Nature 526, 666–671, doi:10.1038/nature15541 (2015). [PubMed: 26375259]
27. Vanden Berghe T, Linkermann A, Jouan-Lanhouet S, Walczak H & Vandenabeele P Regulated necrosis: the expanding network of non-apoptotic cell death pathways. Nat Rev Mol Cell Biol 15, 135–147, doi:10.1038/nrm3737 (2014). [PubMed: 24452471]
28. Filiano AJ, Gadani SP & Kipnis J How and why do T cells and their derived cytokines affect the injured and healthy brain? Nat Rev Neurosci 18, 375–384, doi:10.1038/nrn.2017.39 (2017). [PubMed: 28446786]
29. Hammond TR, Robinton D & Stevens B Microglia and the Brain: Complementary Partners in Development and Disease. Annu Rev Cell Dev Biol 34, 523–544, doi:10.1146/annurev-cellbio-100616-060509 (2018). [PubMed: 30089221]

30. Subba Rao K Mechanisms of disease: DNA repair defects and neurological disease. Nat Clin Pract Neurol 3, 162–172, doi:10.1038/ncpneuro0448 (2007). [PubMed: 17342192]
31. Kuida K et al. Altered cytokine export and apoptosis in mice deficient in interleukin-1 beta converting enzyme. Science 267, 2000–2003 (1995). [PubMed: 7535475]
32. Kovarova M et al. NLRP1-dependent pyroptosis leads to acute lung injury and morbidity in mice. J Immunol 189, 2006–2016, doi:10.4049/jimmunol.1201065 (2012). [PubMed: 22753929]
33. Hou B, Reizis B & DeFranco AL Toll-like receptors activate innate and adaptive immunity by using dendritic cell-intrinsic and -extrinsic mechanisms. Immunity 29, 272–282, doi:10.1016/j.immuni.2008.05.016 (2008). [PubMed: 18656388]
34. Glaccum MB et al. Phenotypic and functional characterization of mice that lack the type I receptor for IL-1. J Immunol 159, 3364–3371 (1997). [PubMed: 9317135]
35. Hoshino K et al. Cutting edge: generation of IL-18 receptor-deficient mice: evidence for IL-1 receptor-related protein as an essential IL-18 binding receptor. J Immunol 162, 5041–5044 (1999). [PubMed: 10227969]
36. Wang S et al. Murine caspase-11, an ICE-interacting protease, is essential for the activation of ICE. Cell 92, 501–509, doi:10.1016/s0092-8674(00)80943-5 (1998). [PubMed: 9491891]
37. Case CL et al. Caspase-11 stimulates rapid flagellin-independent pyroptosis in response to Legionella pneumophila. Proc Natl Acad Sci U S A 110, 1851–1856, doi:10.1073/pnas.1211521110 (2013). [PubMed: 23307811]
38. Tronche F et al. Disruption of the glucocorticoid receptor gene in the nervous system results in reduced anxiety. Nat Genet 23, 99–103, doi:10.1038/12703 (1999). [PubMed: 10471508]
39. Yona S et al. Fate mapping reveals origins and dynamics of monocytes and tissue macrophages under homeostasis. Immunity 38, 79–91, doi:10.1016/j.immuni.2012.12.001 (2013). [PubMed: 23273845]
40. Chen SH, Oyarzabal EA & Hong JS Preparation of rodent primary cultures for neuron-glia, mixed glia, enriched microglia, and reconstituted cultures with microglia. Methods Mol Biol 1041, 231–240, doi:10.1007/978-1-62703-520-0_21 (2013). [PubMed: 23813383]

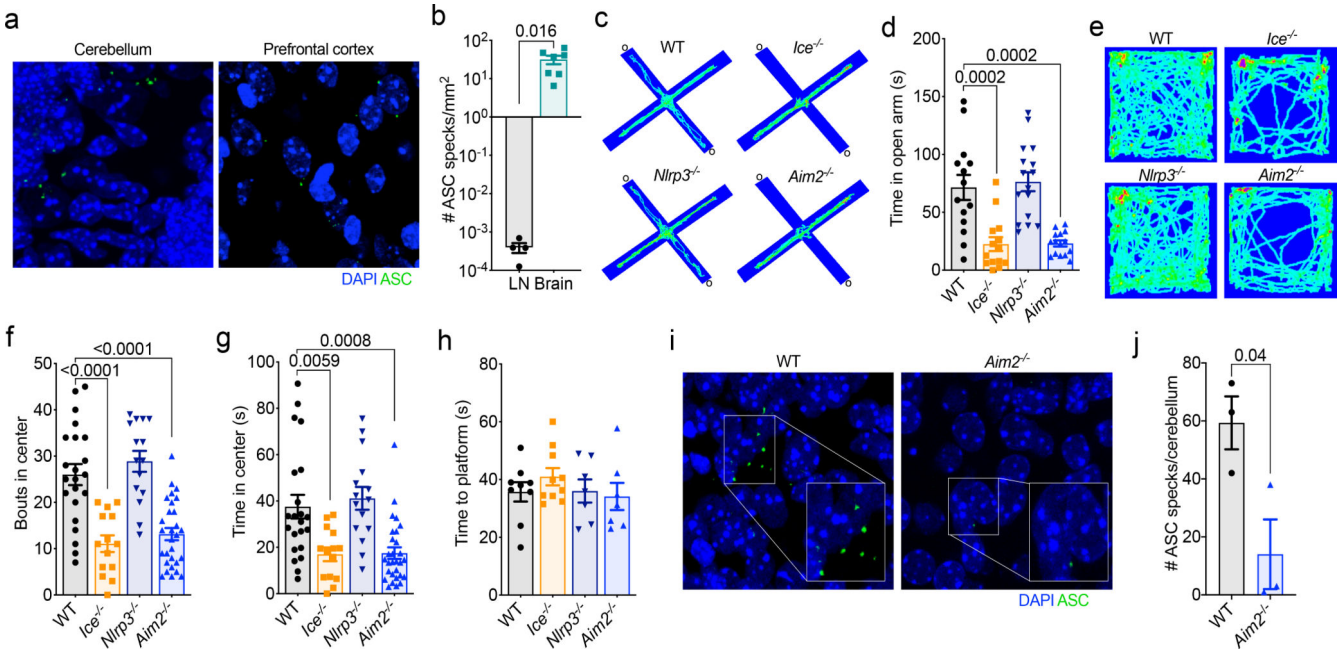

Figure 1. Inflammasome activation occurs in the CNS during neurodevelopment and disruption of the AIM2 inflammasome results in anxiety-related behaviors.

(a) Brains from postnatal day 5 (p5) ASC-Citrine reporter mice were analyzed for the presence of ASC specks (green). Representative images from 3 independent experiments with similar results. (b) Number of ASC specks formed in the brain at p5 (n=7; from 3 independent experiments) and the adult (8–16 weeks old) deep cervical lymph nodes (DCLN) (n=4; representative data from 2 independent experiments). (c-h) Wild-type (WT), *Ice*$^{-/-}$, *Nlrp3*$^{-/-}$, and *Aim2*$^{-/-}$ mice (8–12 weeks old) were assessed for behavioral abnormalities. (c-g) Anxiety behaviors were assessed using the elevated plus maze and the open field test. (c) Representative elevated plus maze heat maps; open arms (o); from 6 independent experiments with similar results. (d) Quantification of time spent in the open arms of the elevated plus maze (WT n=14, *Ice*$^{-/-}$ n=14, *Nlrp3*$^{-/-}$ n=16, *Aim2*$^{-/-}$ n=15; from 3 independent experiments). (e) Representative open field arena heat maps; from 6 independent experiments with similar results. (f-g) Quantification of (f) bouts into and (g) time spent in the center of the open field arena (WT n=22, *Ice*$^{-/-}$ n=14, *Nlrp3*$^{-/-}$ n=15, *Aim2*$^{-/-}$ n=29; from 5 independent experiments). (h) Visual platform test of the Morris water maze (WT n=9, *Ice*$^{-/-}$ n=10, *Nlrp3*$^{-/-}$ n=7, *Aim2*$^{-/-}$ n=7; from 2 independent experiments). (i-j) Cerebellar ASC speck formation in p5 WT and *Aim2*$^{-/-}$ mice. (i) Representative images from 2 independent experiments with similar results. (j) Quantification of cerebellar ASC speck formation in WT n=3 and *Aim2*$^{-/-}$ n=3 mice; representative data from 2 independent experiments. All n values refer to the number of mice used. Error bars depict mean ± s.e.m. Statistics calculated by unpaired two-tailed Student's t-test (b,j) or one-way ANOVA with Tukey's post hoc tests (d,f,g,h).

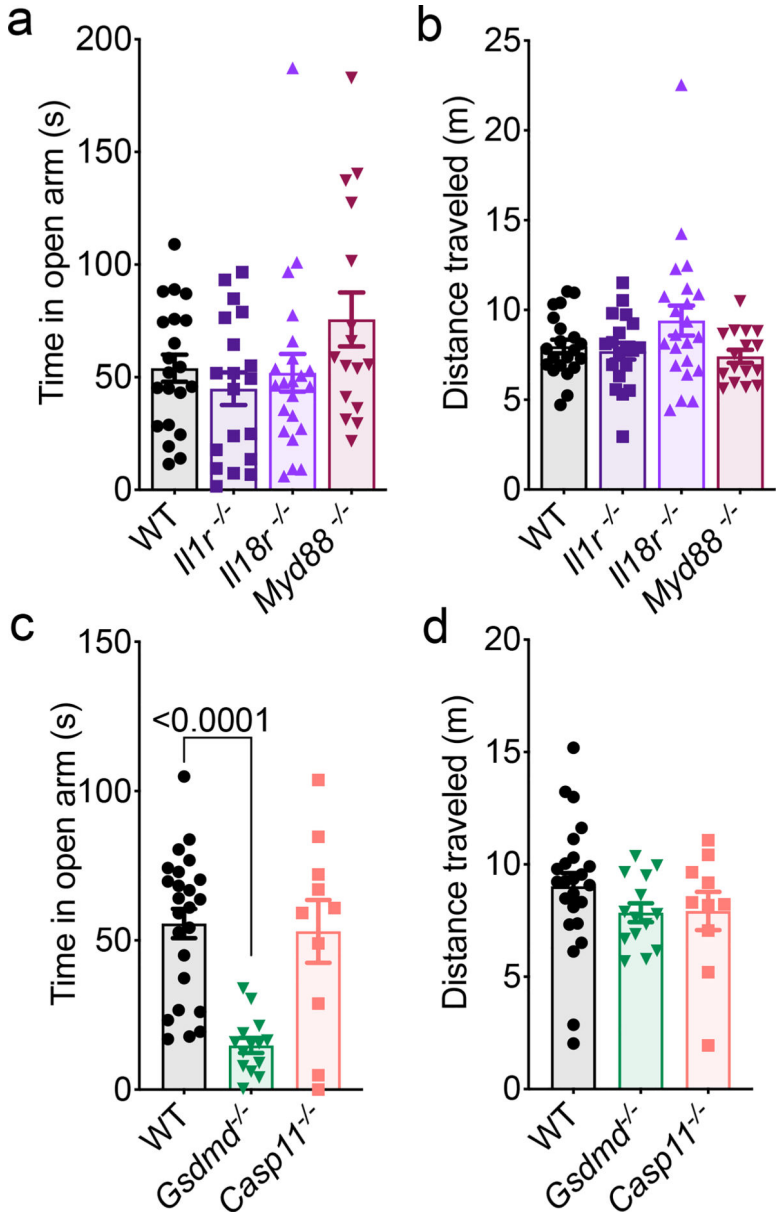

Figure 2. Lack of Gasdermin-D activation drives anxiety-like behaviors in mice.

(a-d) Anxiety-related behaviors were assessed in adult (8–12 weeks old) WT, *Il1r*$^{-/-}$, *Il18r*$^{-/-}$, *Myd88*$^{-/-}$, *Gsdmd*$^{-/-}$, and *Casp11*$^{-/-}$ mice using the elevated plus maze. (a-b) Quantification of (a) time spent in the open arms (o) and (b) distance traveled (WT n=21, *Il1r*$^{-/-}$ n=19, *Il18r*$^{-/-}$ n=22, *Myd88*$^{-/-}$ n=16; from 4 independent experiments). (c) Time spent in the open arms of the elevated plus maze and (d) total distance traveled during testing (WT n=24, *Gsdmd*$^{-/-}$ n=14, *Casp11*$^{-/-}$ n=10; from 2 independent experiments). All n values refer to the number of mice used. Error bars depict mean ± s.e.m. Statistics calculated by one-way ANOVA with Tukey's post hoc tests.

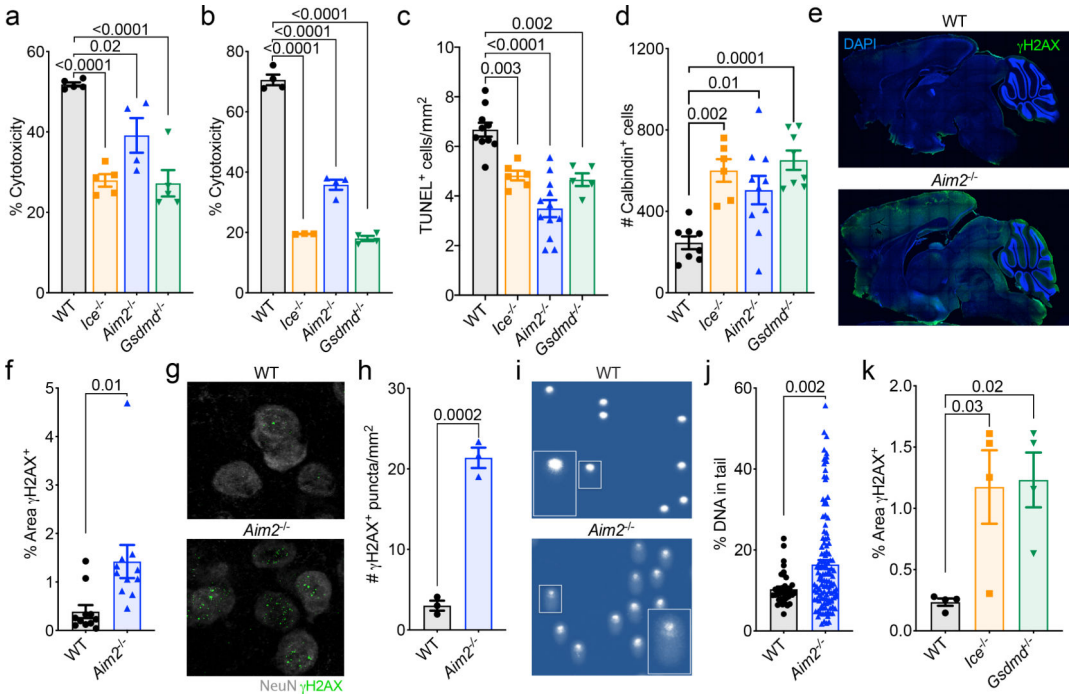

Figure 3. Activation of the AIM2 inflammasome in response to DNA damage coordinates CNS cell death and limits the accumulation of DNA damage in the brain.

(a-b) Postnatal day 0 (p0) mixed neural cultures were primed with LPS for 4 hrs followed by overnight treatment with either (a) 40 Gy ionizing radiation (WT *n*=5, *Ice*$^{-/-}$ *n*=5, *Aim2*$^{-/-}$ *n*=4, and *Gsdmd*$^{-/-}$ *n*=5) or (b) 100 μM etoposide (WT *n*=4, *Ice*$^{-/-}$ *n*=3, *Aim2*$^{-/-}$ *n*=4, and *Gsdmd*$^{-/-}$ *n*=4). Cell death was measured by LDH release. Representative data from 3 independent experiments. (c) Quantification of cerebellar TUNEL staining in p5 mice (WT *n*=10, *Ice*$^{-/-}$ *n*=6, *Aim2*$^{-/-}$ *n*=12, and *Gsdmd*$^{-/-}$ *n*=5 mice; from 3 independent experiments). (d) Enumeration of cerebellar calbindin^{+} Purkinje neurons in adult (8–12 weeks old) mice (WT *n*=8, *Ice*$^{-/-}$ *n*=6, *Aim2*$^{-/-}$ *n*=10, and *Gsdmd*$^{-/-}$ *n*=8 mice; from 3 independent experiments). (e-f) Adult brains were evaluated for levels of DNA damage (γH2AX, green). (e) Representative images from 3 independent experiments with similar results. (f) Quantification of γH2AX staining in adult mice (WT *n*=11, *Aim2*$^{-/-}$ *n*=11; from 3 independent experiments). (g-h) Adult brains were evaluated for γH2AX staining in NeuN-expressing neurons in the amygdala. (g) Representative images from 2 independent experiments with similar results. (h) Enumeration of γH2AX puncta in the amygdala (WT *n*=3, *Aim2*$^{-/-}$ *n*=3; representative data from 2 independent experiments). (i-j) DNA damage was evaluated in the cortex of 10-week-old WT and *Aim2*$^{-/-}$ mice by comet assay. (i) Representative images of single cell electrophoresis gels from 3 independent experiments with similar results. (j) Quantification of percent DNA in tail (WT *n*=38, *Aim2*$^{-/-}$ *n*=120; from 3 independent experiments). (k) Quantification of γH2AX staining in sagittal brain sections from WT *n*=4, *Ice*$^{-/-}$ *n*=4, and *Gsdmd*$^{-/-}$ *n*=4 mice; from 2 independent experiments. Error bars depict mean ± s.e.m. Statistics calculated by (a-d,k) one-way ANOVA with Tukey's post hoc tests and (f,h,j) unpaired two-tailed Student's *t*-test. (a-b,j) *n* values refer to biological replicates from representative experiments. (c-d,f,h,k) *n* values refer to the number of mice used.

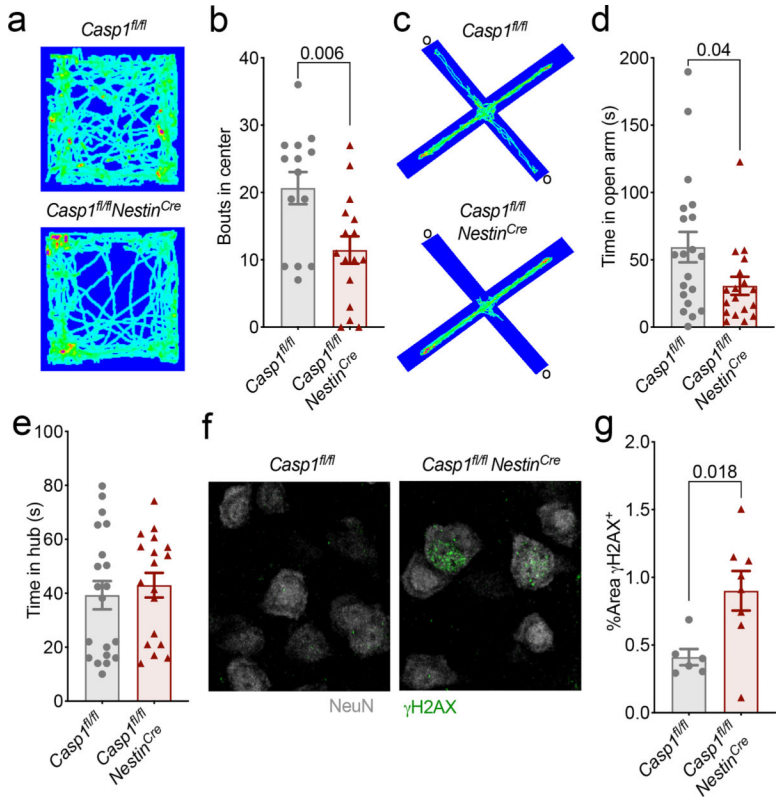

Figure 4. CNS-specific deletion of Caspase-1 results in anxiety-like behaviors and DNA damage accumulation in the brain.

(a-e) Anxiety-associated behaviors were assessed in adult (8–12 weeks old) *Casp1*$^{fl/fl}$ and *Casp1*$^{fl/fl}$*Nestin*^{Cre} mice. (a) Representative heat maps of the path mice traveled in the open field arena; from 3 independent experiments with similar results. (b) Quantification of bouts into the center of the open field arena (*Casp1*$^{fl/fl}$ *n=14, Casp1*$^{fl/fl}$*Nestin*^{Cre} *n*=16; from 3 independent experiments). (c) Representative heat maps depicting path of travel through open arms (o) and closed arms of the elevated plus maze; from 4 independent experiments with similar results. (d) Quantification of time spent in the open arms of the elevated plus maze and (e) time in the hub (*Casp1*$^{fl/fl}$ *n=20, Casp1*$^{fl/fl}$*Nestin*^{Cre} *n*=18; from 4 independent experiments). (f-g) Adult brains were evaluated for levels of DNA damage (γH2AX, green) in NeuN-expressing neurons. (f) Representative cortex images from 2 independent experiments with similar results. (g) Quantification of γH2AX staining in cortical brain sections (*Casp1*$^{fl/fl}$ *n*=6 and *Casp1*$^{fl/fl}$*Nestin*^{Cre} *n*=8; from 2 independent experiments). All *n* values refer to the number of mice used. Error bars depict mean ± s.e.m. Statistics calculated by unpaired two-tailed Student's *t*-test.